

Structural, optical and room temperature ferromagnetic properties of $\text{Sn}_{1-x}\text{Fe}_x\text{O}_2$ thin films using flash evaporation technique

M. Kuppan¹ · S. Kaleemulla¹ · N. MadhusudhanaRao¹ · C. Krishnamoorthi¹ · I. Omkaram² · D. SreekanthaReddy³

Received: 21 April 2016 / Accepted: 11 October 2016 / Published online: 18 October 2016
© Springer Science+Business Media New York 2016

Abstract Iron doped tin oxide thin films ($\text{Sn}_{1-x}\text{Fe}_x\text{O}_2$) at $x = 0.00, 0.03, 0.05, 0.07, 0.10$ and 0.15 were prepared onto Corning 7059 substrates using flash evaporation technique and studied the effect of iron (Fe) doping concentration on structural, optical and magnetic properties of the prepared thin films. From the X-ray diffraction patterns, it was found that the $\text{Sn}_{1-x}\text{Fe}_x\text{O}_2$ thin films were polycrystalline with tetragonal structure. The crystallite sizes of the films were calculated using Scherrer's relation and found that it was about 25 nm. The chemical composition and oxidation states of the elements were found using energy dispersive analysis of X-rays and X-ray photoelectron spectroscopy. From this it was confirmed that the Fe was substituted Sn sites and is in Fe^{+3} states. The optical band gap of the films decreased from 3.98 to 3.76 eV with increase of Fe doping concentration. The pure SnO_2 thin films exhibited diamagnetism whereas $\text{Sn}_{1-x}\text{Fe}_x\text{O}_2$ thin films exhibited ferromagnetism at room temperature. A magnetic (M_s), coercivity (H_{ci}) and retentivity (M_r) were found to be 13.062 emu/cm^3 , 114.98 G , $7.487 \times 10^{-6} \text{ emu/cm}^3$, respectively $\text{Sn}_{1-x}\text{Fe}_x\text{O}_2$ thin films at $x = 0.07$.

1 Introduction

Conversion of a non-magnetic semiconductor into magnetic semiconductor by doping small quantities of transition metal ions is called as dilute magnetic semiconductors (DMS). Recently these DMS materials have received more attention due to their potential applications in spin based electronics or called as spintronics devices [1] in which both spin and charge of electron can be utilized [1]. An important property that a DMS should possess is the realization of ferromagnetism with Curie temperature near or above room temperature. Since the prediction of room temperature ferromagnetism (RTFM) in Mn doped ZnO and GaN, extensive studies were carried out on wide band gap oxide semiconductor to achieve ferromagnetism at room temperature [2]. Till today different wide band gap oxide semiconductors such as zinc oxide, titanium dioxide, indium oxide and tin oxide were studied for room temperature ferromagnetism [3–6]. Among these oxides, SnO_2 is a n-type, rutile structure semiconductor with a band gap of 3.6 eV [7]. It is transparent in the visible region and reflective in the infrared region [8]. Due to its high optical transmittance and high electrical conductivity, it find in many applications such as such as optoelectronic and photo voltaic devices, light emitting and light triggered devices, transparent conducting plate in solar cells, liquid crystal displays, plasma display panels, touch screens and solid state gas sensors, etc. [9–12]. Since it is known that the magnetic interactions in dilute magnetic semiconductors are generally thought as charge carrier mediated, SnO_2 sees to be a promising candidate as a host oxide semiconductor for DMS. The undoped and transition metal doped SnO_2 is particularly interesting in the field of DMS due to its high optical transparency and chemical sensitivity and has been studied extensively by many research groups [13–15].

✉ S. Kaleemulla
skaleemulla@gmail.com

¹ Thin Films Laboratory, Centre for Crystal Growth, VIT University, Vellore 632014, Tamilnadu, India

² Department of Electronics and Radio Engineering, Kyung Hee University, Yongin-si, Gyeonggi-do 441-701, South Korea

³ Department of Physics and Sungkyukwan Advanced Institute of Nanotechnology (SAINT), Sungkyunkwan University, Suwan 440746, Korea

Torres et al. [16] deposited Fe doped SnO₂ thin films onto LaAlO₃ substrates using pulsed laser deposition (PLD) technique and reported that both pure and Fe doped SnO₂ thin films were ferromagnetic in nature. In this the pure SnO₂ films exhibited the saturation magnetization of 33 emu/cm³ (3.6 emu/g). It was confirmed that the reason for the observed ferromagnetism in pure SnO₂ thin films was due to shape of the substrates or defects formed during the preparation of the films. Coey et al. [17]. deposited Fe doped SnO₂ thin films onto R-cut sapphire substrate using PLD technique and reported that Sn_{0.95}Fe_{0.05}O₂ films were ferromagnetic with Curie temperature and saturation magnetization of 610 K and 2.2 Am²kg⁻¹. Ferromagnetic coupling of ferric ions via electron trapped in a bridging oxygen vacancy (F-center) model was proposed to explain high Curie temperature in the films.

Fitzgerald et al. [18] prepared Fe doped SnO₂ thin films onto R-cut sapphire substrate using PLD technique and reported that the Sn_{0.85}Fe_{0.15}O₂ films were ferromagnetic at room temperature with saturation magnetization of 7 × 10⁻⁸ Am² and concluded that much of the magnetic moment was associated with electronic defects or lattice defects which might be present in thinnest films. Recently Chandra et al. [19]. prepared both undoped, and (Fe, F) co-doped SnO₂ thin films onto glass substrates using a simplified spray pyrolysis technique. The room temperature ferromagnetism was confirmed in all the samples. The ferromagnetic behavior is found to increase with Fe doping concentration. Ghanaatshoar et al. [20] deposited Fe doped SnO₂ thin films by two different methods using electron beam evaporation technique. In the first procedure, which is the common one, each deposition target was prepared by mixing SnO₂ and Fe powders and, in the second one, tin oxide and iron targets were prepared separately. It has been revealed that Fe islands have been formed in the films which were produced by the second method. These thin layers also manifested ferromagnetic properties, while those which were deposited by the first procedure were not capable of yielding room-temperature ferromagnetism. To the best of author's knowledge less work was reported on Fe doped SnO₂ thin films using flash evaporation technique. Hence an attempt is made here to prepare Fe doped SnO₂ thin films at different Fe doping concentrations and studied the doping influence on structural, optical and magnetic properties of the films. Though few reports are available on transition metal doped SnO₂ DMS, the origin of the room temperature ferromagnetism is not clear. Hence an attempt is made here to prepare iron doped tin oxide thin films using flash evaporation technique and studied the effect of Fe doping concentration on structural, optical and magnetic properties of the prepared films.

2 Experimental

The target material Fe doped SnO₂ fine powder was prepared using solid state reaction as discussed elsewhere [21]. The same powder was used here for the preparation of Fe doped SnO₂ thin films. Fe doped SnO₂ thin films were grown on glass substrates using the flash evaporation technique. The system is capable of producing an ultimate vacuum of 5 × 10⁻⁶ mbar. The vacuum chamber was pumped with a diffusion pump and a rotary pump combination. The pressure in the vacuum chamber was measured using digital pirani and penning gauge combination. A resistively heated molybdenum boat was used for the quick evaporation of the charge material. The temperature of the molybdenum boat was maintained at a temperature sufficiently higher than the melting points of the individual evaporants. The resistively heated molybdenum boat was used at a temperature sufficiently high enough to evaporate the material instantaneously. Here small grains of the evaporant alloys were dropped slowly into the hot boat which immediately get vaporizes to form a condensate on nearby heated substrate, ensuring the stoichiometry of the films. This high temperature causes simultaneous vaporization of the material and also imparts sufficient kinetic energy to the particles in the vapour phase. During the deposition the evaporant powder was dropped slowly into the hot molybdenum boat by means of an electrophonically operated hopper. The feeding rate was maintained constant till the end of deposition and the deposition period was typically in the range of 30 min.

Crystallinity and structural properties of the films were studied by X-ray diffraction technique (X-ray diffractometer D8 Advance, BRUKER) using Cu K α radiation. Optical transmittance spectra were recorded using UV–VIS spectrophotometer (JASCO-V-670) in the wavelength range of 200–2500 nm. The surface morphology of the films was studied by field emission scanning electron microscopy (FESEM, Carl Zeiss, EVO MA 15) and the composition of the films were studied by using energy dispersive spectroscopy, (OXFORD instrument INCA penta FET X3). X-ray photoelectron spectroscopy (XPS) was employed to determine the composition and valence state of the element of the films using VG ESCALAB MK II. Magnetic properties of the films were studied through magnetic field dependent magnetization (hysteresis) loops up to 1 T field at room temperature by calibrated vibrating sample magnetometer (Lake Shore 7404). The magnetic field is applied perpendicular to the surface of the films (out of plane configuration) and a magnetic hysteresis loop of bare substrate was also measured for subtraction purpose.

3 Results and discussion

3.1 Structural properties

Figure 1a shows the X-ray diffraction profiles of bulk Fe_2O_3 and SnO_2 . In the figure the top layer indicate the X-ray diffraction profiles of bulk Fe_2O_3 . It shows the characteristic diffraction peaks at an angles $2\theta = 24.16^\circ$, 33.11° , 35.62° , 40.86° , 49.46° , 54.11° , 57.60° , 62.34° , 64.02° , 71.89° and 75.34° , are assigned to the scattering from (0 1 2), (1 0 4), (1 1 0), (1 1 3), (0 2 4), (1 1 6), (0 1 8), (2 1 4), (3 0 0). All the diffraction peaks of Fe_2O_3 spectrum are in good accordance with a hexagonal type - Fe_2O_3 (JCPDS card no. 33-664) [22]. The bottom layer of Fig. 1a shows the X-ray diffraction profiles of bulk SnO_2 . The diffraction peaks were found at diffraction angles of 26.62° (1 1 0), 33.89° (1 0 1), 37.98° (2 0 0), 39.09° (1 1 1), 42.65° (2 1 0), 51.80° (2 1 1), 54.79° (2 2 0), 57.85° (0 0 2), 61.92° (3 1 0), 64.75° (1 1 2), 65.98° (3 0 1), 71.39° (2 0 2), and 78.73° (3 2 1) were exactly coincided with tetragonal structure of SnO_2 [JCPDS No. 411445]. Crystal phases related to Fe metal clusters and Fe_2O_3 were found in XRD patterns of Fe doped SnO_2 thin films at $x = 10$ and $15 \text{ at.}\%$. Similarly in XRD profile of SnO_2 no other phases of tin such as Sn metal clusters or SnO were found. From these XRD profiles it confirms that the host and dopant materials are free from other impurity phases.

Figure 1b shows the X-ray diffraction patterns of $\text{Sn}_{1-x}\text{Fe}_x\text{O}_2$ thin films at different Fe doping concentrations. The diffraction peaks such as (1 1 0), (1 0 1), (2 0 0), (2 1 1) and (2 2 0) of SnO_2 was observed in the films. Among, the different orientations the (1 1 0) was more predominant. All the diffracted peaks of thin films exactly coincided with the tetragonal structure of SnO_2 (JCPDS data No: 41-1445). No other peaks were detected which are related to either Fe or Fe_2O_3 in $\text{Sn}_{1-x}\text{Fe}_x\text{O}_2$ up to ($x = 0-0.07$) thin films. No significant change in the diffracted angle was found when the Fe doping concentration was increased.

The average crystallite size (L) was calculated by using the Scherer's relation [23],

$$L = k\lambda/\beta \cos \quad (1)$$

where, k is a constant, λ is the wavelength of Cu K_α ($\lambda = 1.5406 \text{ \AA}$) used in X-ray diffraction, β is the Full width at half maximum, θ is the diffracted angle respectively. The average crystallite sizes of $\text{Sn}_{1-x}\text{Fe}_x\text{O}_2$ samples were found to be 24 nm.

Figure 1c shows the XRD patterns of the $\text{Sn}_{1-x}\text{Fe}_x\text{O}_2$ thin films at $x = 0.10$ and $x = 0.15$ Fe doping concentrations. From the figure it is clear that the peaks were related to SnO_2 along with iron metal clusters and Fe_2O_3 . Here also the diffraction peaks related to tin oxide were observed

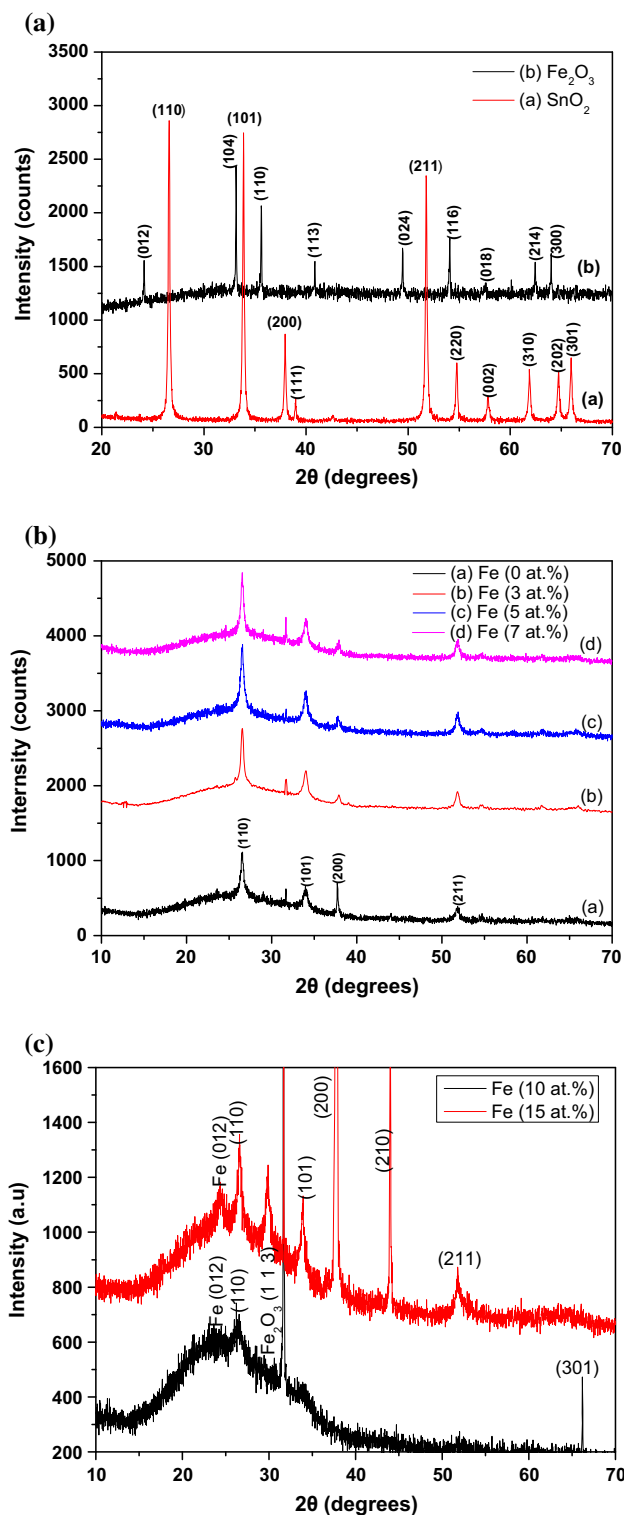


Fig. 1 a X-ray diffraction patterns of precursor SnO_2 , Fe_2O_3 . b X-ray diffraction patterns of $\text{Sn}_{1-x}\text{Fe}_x\text{O}_2$ thin films at different 'x'. c X-ray diffraction patterns of $\text{Sn}_{1-x}\text{Fe}_x\text{O}_2$ thin films at $x = 0.10$ and $x = 0.15$

and found that the predominant orientation was due to SnO_2 only. Also the plane (2 0 0) was found to be predominant diffraction peak. But in addition to the SnO_2

planes, a diffraction peak related to Fe in (0 1 2) at diffraction angle of 24° was also found in the Fe at 10 and 15 at.%. The intensity of the diffraction peaks increased at higher doping concentrations. But the secondary phases related to impurities were not found in Co/Li doped SnO_2 thin films also when the doping concentration increased from 0 to 15 at.% [16, 24, 25]. But in our present study Fe phase was found from the XRD. The lattice constant of the films decreased with increase of doping concentration. The lattice constant decreased from 4.746 to 4.735 Å with increase of doping concentration from 0 to 15 at.%. It may be due to difference in the ionic radius of iron and tin.

3.2 Composition and surface studies

Figure 2a, b show the energy dispersive analysis of X-rays (EDAX) spectra of $\text{Sn}_{1-x}\text{Fe}_x\text{O}_2$ thin films at $x = 0.05$ and 0.07 doping concentrations. From this it is confirmed that the impurity ion Fe was substituted in SnO_2 lattice. From the EDAX spectra it was found that the compositions of the elements such iron (Fe), tin (Sn) and oxygen (O) were almost equal to that of that of target composition. For

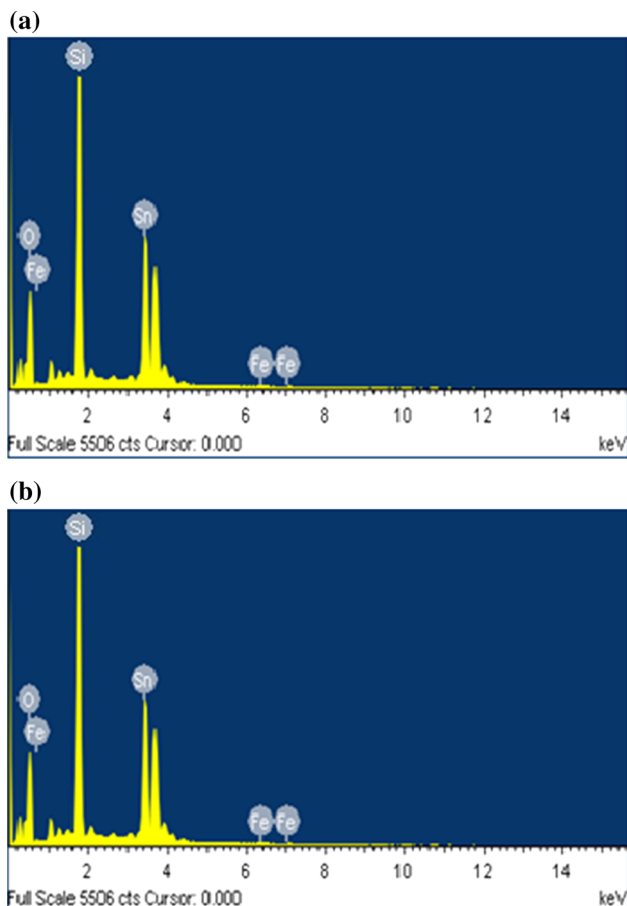


Fig. 2 **a** EDAX spectrum of $\text{Sn}_{1-x}\text{Fe}_x\text{O}_2$ thin films at $x = 0.05$. **b** EDAX spectrum of $\text{Sn}_{1-x}\text{Fe}_x\text{O}_2$ thin films at $x = 0.07$

example, the elements Fe, Sn and O were found to be 50.30, 4.47 and 45.26 at.% for $\text{Sn}_{1-x}\text{Fe}_x\text{O}_2$ thin films at $x = 0.05$. No additional impurities were found in the EDAX spectra indicating that the observed room temperature ferromagnetism is not due to any other impurities.

Figure 3a, b shows the FE-SEM images of $\text{Sn}_{1-x}\text{Fe}_x\text{O}_2$ thin films at $x = 0.07$ and 0.15. From the images it is clear that the films consist of grain of different sizes in almost spherical in shape. The average particle size was estimated and is found to be about 80 nm which is larger than that of crystallite size calculated from X-ray diffraction. The grain size increased with increase of doping concentration. It may be due to synthesis condition which might affect the grain size of the particles.

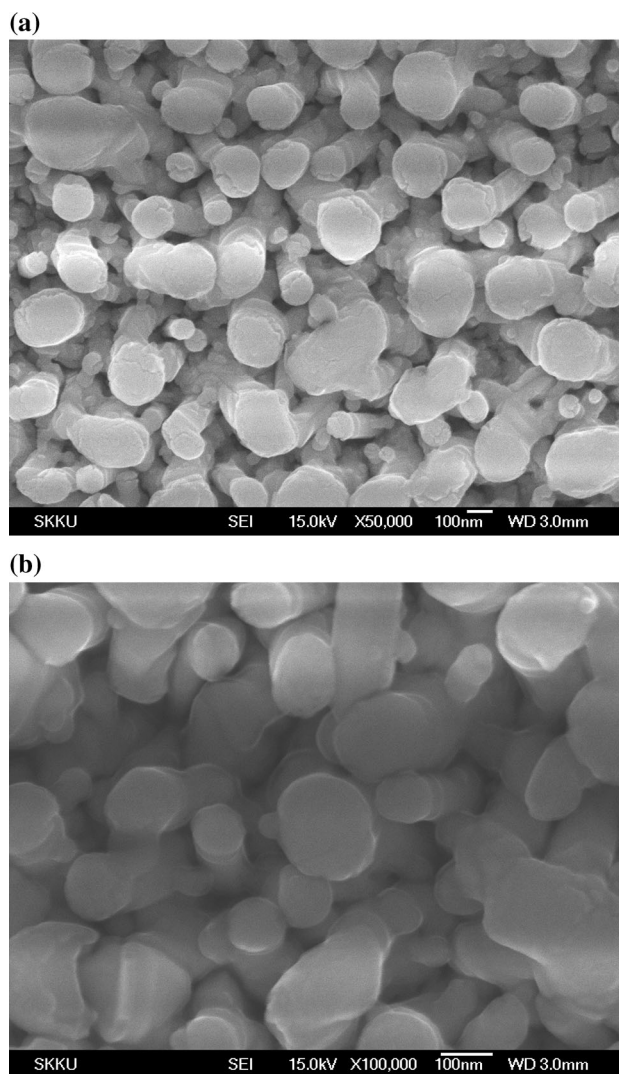


Fig. 3 **a** FE-SEM micrograph of the $\text{Sn}_{1-x}\text{Fe}_x\text{O}_2$ thin films at $x = 0.07$. **b** FE-SEM micrograph of $\text{Sn}_{1-x}\text{Fe}_x\text{O}_2$ thin films at $x = 0.15$

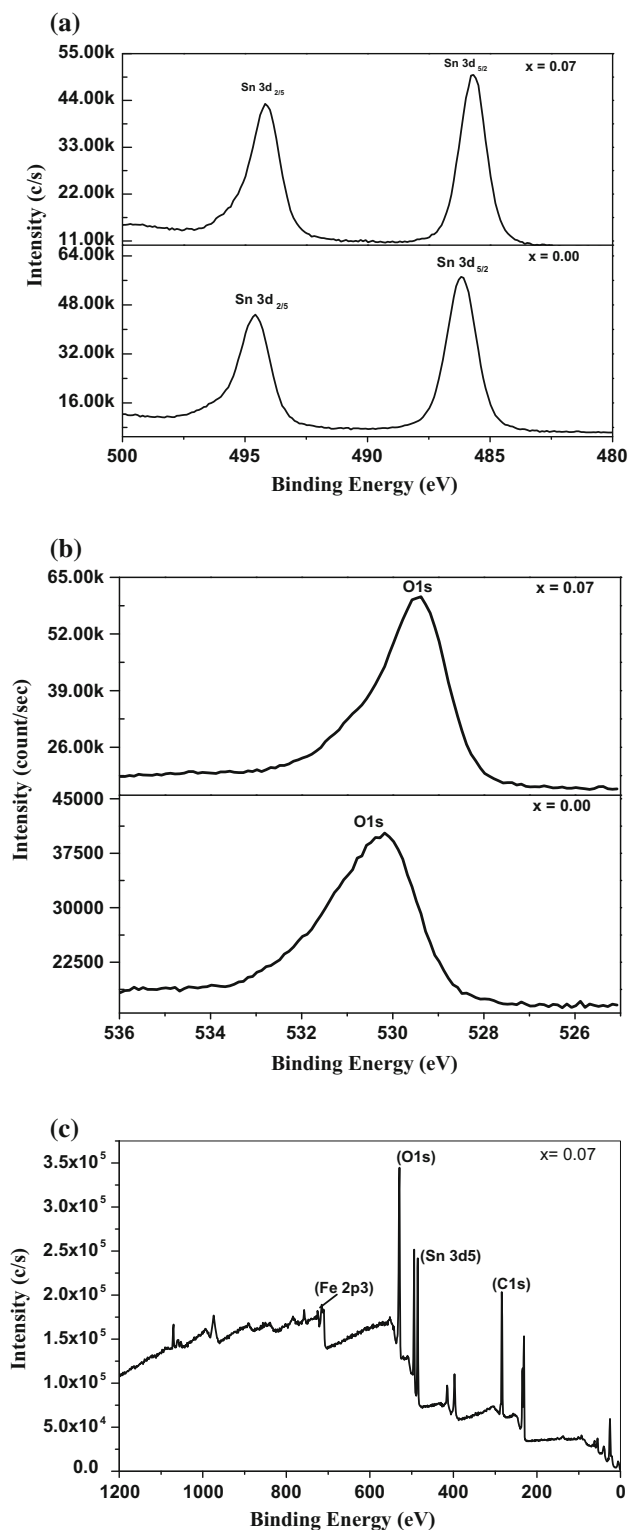


Fig. 4 **a** XPS spectra of Sn_{3d} edge of Sn_{1-x}Fe_xO₂ thin films at $x = 0.00$ and 0.07. **b** XPS spectra of O1s edge of Sn_{1-x}Fe_xO₂ thin films at $x = 0.00$ and 0.07. **c** XPS survey scan spectra of Sn_{1-x}Fe_xO₂ thin films at $x = 0.07$

3.3 XPS studies

Figure 4a XPS spectra of Sn3d edge of Sn_{1-x}Fe_xO₂ thin films at $x = 0.00$ and 0.07. As shown in Fig. 4a, the double spectral lines of Sn3d appears at binding energies of 486.14 (Sn 3d_{5/2}) and 494.62 eV (Sn3d_{3/2}), with a spin-orbit splitting of 8.48 eV [24]. Further the Sn 3d_{5/2} peak shows only one symmetric component without a shoulder peak, indicating the absence of Sn²⁺ ions. Fig. 4b shows a highly symmetric O 1s peak centered at 530.28 eV, corresponding to the lattice oxygen (O- Sn bonds) [25]. A shift of 0.09 eV in the O1s core-level position was observed in the film when Fe concentration increased from $x = 0.00$ –0.07. Such a shift may be attributed to increase in oxygen vacancies in the samples. Figure 4c shows the survey scan spectrum of Sn_{1-x}Fe_xO₂ thin films at 0.07. The binding energy of Fe 2p_{3/2} is 710.4 eV, which excludes the formation of Fe clusters since the binding energy of Fe 2p_{3/2} for Fe is 706.7 eV. The presence of Fe²⁺ ions is due to the partial reduction of Fe³⁺ when the O ions locating close to the Fe sites were partially replaced by Sn ions. The peaks observed at 710.72 and 724.22 eV in correspond to the binding energy of Fe 2p_{3/2} and 2p_{1/2}, respectively [26]. No additional peaks corresponding to Fe metal clusters are noticed in any of the spectra. Combined with the higher energy shifting trend of shake-up satellite peaks lie between Fe 2p_{1/2} and Fe 2p_{3/2}, it's confirmed that the Fe dopants are all +3 valence.

3.4 Optical properties

Figure 5a shows the optical transmittance spectra of undoped and Fe doped SnO₂ thin films. From the figure it is clear that both undoped and Fe doped SnO₂ thin films were exhibiting transmittance more than 85 % at higher wavelengths and less transmittance in the visible region. Particularly interference fringes can be seen for both undoped and Fe doped SnO₂ thin films. It may be due to high surface roughness of the films which can produce more scattering centers [27].

The optical band gap (E_g) for highly degenerate semi-conducting oxides can be determined from the absorption coefficient (α) and photon energy ($h\nu$) using Tauc's relation [28]

$$\alpha h\nu = A (E_g - h\nu)^{1/2} \quad (2)$$

The optical band gap E_g is obtained by plotting $(\alpha h\nu)^2$ versus the photon energy ($h\nu$) and by extrapolating the linear region of the plots to zero absorption ($\alpha = 0$). The undoped SnO₂ films exhibited an optical band gap of

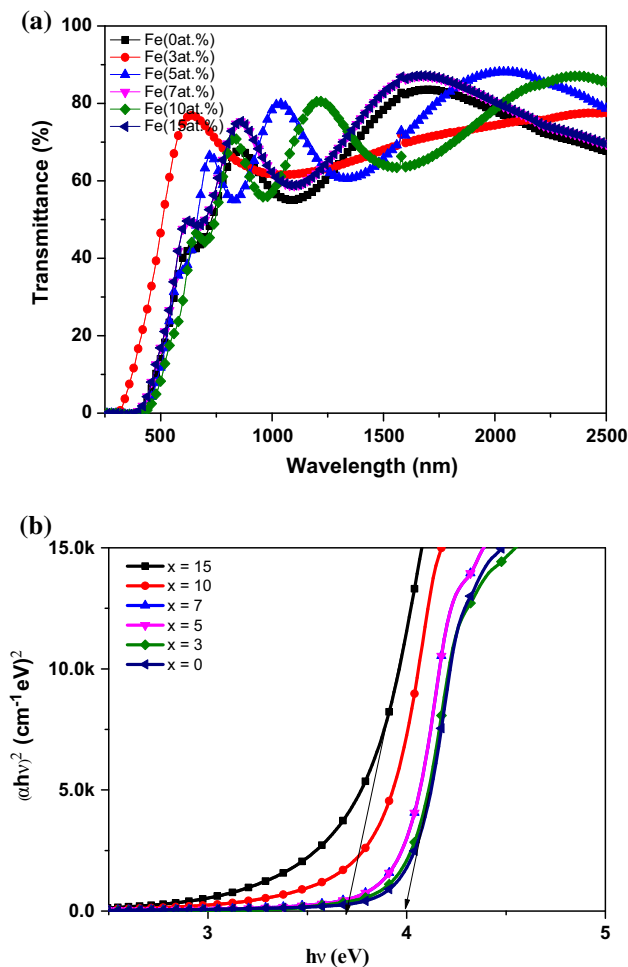


Fig. 5 **a** Optical transmittance spectra of $\text{Sn}_{1-x}\text{Fe}_x\text{O}_2$ thin films at different Fe doping concentrations. **b** Plots of $(\alpha hv)^2$ versus photon energy ($h\nu$) for $\text{Sn}_{1-x}\text{Fe}_x\text{O}_2$ thin films at different 'x'

3.98 eV which is in agreement with the reported value. This kind of behavior was also observed in (Co, Mo) doped SnO_2 thin films [29, 30]. A decrease in optical band gap was observed in Fe doped SnO_2 thin films. The processing parameters such as substrate temperature, crystallite size, crystal defects, particle size distribution and doping concentrations may also affect the optical band gap of the films. Mohagheghi et al. [31] were also noticed the reduction of direct energy gap with Fe^{3+} -doping for SnO_2 thin films prepared by spray pyrolysis technique. The red shift is a commonly observed phenomenon in the transition metal doped II–IV semiconductor and has been attributed to the sp–d spin-exchange interactions between the band electrons and the localized d electrons of the transition-metal ion substituting the cation, where the s–d and p–d exchange interactions could lead to a negative and a positive correction to the conduction-band and the valence-band edges, respectively. In fact, it is also a well-established fact that the variation of band gap due to doping is a result of Moss–Burstein (MB) effect. This shifting of the

absorption edge towards higher wavelengths (red shift) is due to decrease in band gap caused by defects and crystallite size distribution. This red shift has also been reported to be due to incorporation of Fe^{3+} into the SnO_2 crystal structures which leads to the charge-transfer transition between the Fe^{3+} d-electrons and the SnO_2 conduction or valence band [32, 33].

3.5 Magnetic properties

Figure 6a–c shows magnetic field dependence magnetization (hysteresis) loops of $\text{Sn}_{1-x}\text{Fe}_x\text{O}_2$ thin films ($x = 0.0\text{--}0.15$) at room temperature. In order to avoid all these confusion, proper care was taken during the synthesis and characterization of the films. It was reported that the possible ferromagnetism in thin films might be due to contamination by the substrate holder, handling with magnetic tools or the use of some marker pens, tape or sample holders used during the magnetic measurements. Hence in order to avoid such kind of reasons for the observed ferromagnetism, magnetic measurements were also carried out for the blank substrates. Further, we had carried out the magnetic studies for the bare glass substrate which was kept in the deposition chamber under the same deposition conditions without depositing the films. In all these cases we observed diamagnetic nature for the substrates and substrate holders also. Hence it can be considered that the observed ferromagnetism in Fe doped SnO_2 thin films are intrinsic one rather than any impurities. After subtracting the linear diamagnetic background signal, the possible room-temperature ferromagnetism was observed in all samples except for the pure SnO_2 . The diamagnetic nature of undoped SnO_2 converted into ferromagnetic nature by doping Fe into the host material. All the Fe doped thin films exhibited soft ferromagnetic nature with increase of saturation magnetization (M_s). In the literature survey it was mentioned that ferromagnetic nature can be obtained in oxide thin films might be due to magnetic clusters present in the films, or secondary phases present in the films and also due to contamination of the magnetic impurities during preparation or magnetic measurement studies. It is observed that M_s increases with Fe dopant concentration and reaches maximum of 13.06 emu/cm^3 for $x = 0.07$. The magnetization data of the samples were corrected by appropriately subtracting the substrate magnetization data. The diamagnetic nature of bulk SnO_2 was repeated in thin film form also. Generally the thin films of oxide semiconductor exhibits ferromagnetism due to various reasons such as off stoichiometry, defects and oxygen vacancies, etc. The observed diamagnetism may be due to any defects or oxygen vacancies. Room temperature ferromagnetism in bulk and thin films of non-magnetic metal oxides might be caused by defects in present in the system or defects

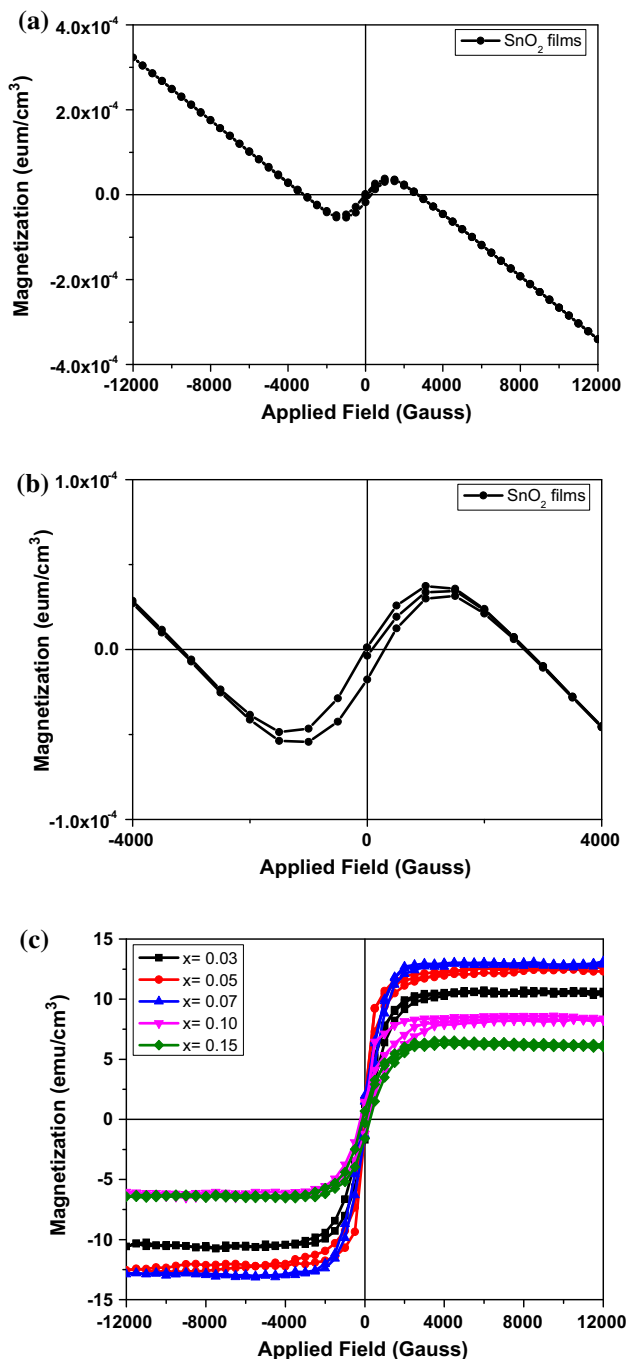


Fig. 6 **a** M–H loop of SnO₂ thin film. **b** Enlarged view of M–H loops SnO₂ thin film in the field range of –4000 G to +4000 G. **c** M–H loops of Sn_{1–x}Fe_xO₂ thin films at $x = 0.03$ – 0.15 . Inset of the figure shows the M–H loop of undoped SnO₂ thin film

created in the system during the preparation of the samples other than transition metal dopants [34–36]. This intrinsic ferromagnetism may arise from magnetic exchange interactions between neighbouring cations via free electrons trapped in anionic vacancies, called F-centered mediated ferromagnetism [37] such a mechanism is widely

thought to be the most relevant to the origin of ferromagnetism in semiconducting oxide thin films as well as oxide based DMS systems.

4 Conclusions

Sn_{1–x}Fe_xO₂ ($x = 0.00$ – 0.15) thin films were successfully prepared on a glass substrates using flash evaporation technique. The influences of doping on structural, optical and magnetic properties of the prepared thin films were studied. The optical band gap of the films decreased with increased doping concentration. The XPS analyses showed an increase of oxygen vacancies with Fe concentration and existence of Fe as Fe(III) state in host SnO₂. The maximum saturation magnetization of Sn_{1–x}Fe_xO₂ films increased with increase of Fe doping concentration. The highest magnetic moment of 13.06 emu/cm³ was found in Fe doped SnO₂ thin films at $x = 0.07$. A decrease in magnetic moment was observed when Fe doping concentration increased to 10 and 15 at. %.

References

1. H. Ohno, *Science* **281**(5379), 951–956 (1998)
2. T. Dietl, H. Ohno, F. Matsukura, J. Cibert, D. Ferrand, *Science* **287**(5455), 1019–1022 (2000)
3. D.Y. Inamdar, A.K. Pathak, I. Dubenko, N. Ali, S. Mahamuni, *J. Phys. Chem. C* **115**, 23671–23676 (2011)
4. R. Suryanarayanan, V.M. Naik, P. Kharel, P. Telagala, R. Naik, *J. Phys. Condens Matter* **17**, 755–762 (2005)
5. C.B. Fitzgerald, M. Venkatesan, A.P. Douvalis, S. Huber, J.M.D. Coey, *J. Appl. Phys.* **95**(11), 7390–7392 (2004)
6. C.B. Fitzgerald, M. Venkatesan, L.S. Dornels, R. Gunning, P. Stamenor, J.M.D. Coey, P.A. Stampe, R.J. Kennedy, E.C. Moreira, U.S. Sias, *Phys. Rev. B* **74**, 115307 (2006)
7. J. Robertson, *Phys. Rev. B* **30**, 3520 (1984)
8. F.J. Yusta, M.L. Hitchman, H. Shamlian, *J. Mater. Chem.* **7**, 1421–1427 (1997)
9. K.L. Chopra, S. Major, D.K. Pandya, *Thin Solid Films* **102**(1), 1–42 (1983)
10. M.W.J. Prins, K.O. Grosse Holz, G. Muller, J.F.M. Cillessen, J.B. Giesberg, R.P. Weening, R.M. Wolf, *Appl. Phys. Lett.* **68**, 3650–3652 (1996)
11. A.V. Tadeev, G. Delabouglise, M. Labeau, *Thin Solid Films* **337**, 163–165 (1999)
12. E. Comini, G. Faglia, G. Sberveglieri, Z.W. Pan, Z.L. Wang, *Appl. Phys. Lett.* **81**, 1869–1871 (2002)
13. A. Punnoose, J. Hays, V. Gopal, V. Shutthanandan, *Appl. Phys. Lett.* **85**, 1559 (2004)
14. K. Nomura, J. Okabayashi, K. Okamura, Y. Yamada, *J. Appl. Phys.* **110**, 083901 (2011)
15. S. Ghosh, M. Mandal, K. Mandal, *J. Magn. Magn. Magn.* **323**, 1083–1087 (2011)
16. C.E.R. Torres, L. Errico, F. Golmar, A.M.M. Navarro, A.F. Cabrera, S. Duhalde, F.H. Sanchez, M. Weissmann, *J. Magn. Magn. Magn.* **316**, 1219–1222 (2007)

17. J.M.D. Coey, A.P. Douvalis, C.B. Fitzgerald, M. Venkatesan, Appl. Phys. Lett. **84**, 1332–1334 (2004)
18. C.B. Fitzgerald, M. Venkatesan, L.S. Dornels, R. Gunning, P. Stamenor, J.M.D. Coey, J. Phy. Rev. B **74**(115307), 1–10 (2006)
19. S. Chandra, K. Ravichandran, G. George, T. Arun, P.V. Ravikumar, J. Mater. Sci. Mater. Electron. **1**, 1–7 (2016)
20. M. Ghanaatshoar, M. Moradi, Z. Khodabandeh, J. Supercond. Nov. Magn. **26**, 995–999 (2013)
21. M. Kuppan, S. Kaleemulla, N. MadhusudhanaRao, N. Sai Krishna, M. RiganaBegam, D. SreekanthaReddy, J. Supercond. Nov Magn. **27**, 1315–1321 (2014)
22. S.T. Navale, S.R. Nalage, M.A. Chougule, S.A. Pawar, V.B. Patil, J. Mater. Sci.-Mater. Electron. **24**(5), 1422–1430 (2013)
23. B.D. Cullity, *Elements of X-ray diffraction* (Addison-Wesley, Reading, 1972)
24. J. Wang, W. Zhou, P. Wu, Appl. Surf. Sci. **314**, 188–192 (2014)
25. S.C. Kashyap, K. Gopinadhan, D.K. Pandya, S. Chaudhary, J. Magn. Magn. Mater. **321**, 957–962 (2009)
26. A.P. Grosvenor, B.A. Kobe, M.C. Biesinger, N.S. McIntyre, Surf. Interface Anal. **36**, 1564–1574 (2004)
27. S. Chacko, N.S. Philips, V.K. Vaidyan, Phys. Stat. Solid A **204**, 3305–3315 (2007)
28. J. Tauc, *Amorphous and liquid semiconductors* (Plenum Press, New York, 1974)
29. S.G. Ansari, M.A. Dar, Y.S. Kim, G.S. Kim, H.K. Seo, G. Khang, H.S. Shin, Appl. Surf. Sci. **253**, 4668–4672 (2007)
30. S. Dalui, S. Rout, A.J. Silvestre, G. Lavareda, L.C.J. Pereira, P. Brogueria, O. Conde, Appl. Surf. Sci. **278**, 127–131 (2013)
31. M. Batzill, U. Diebold, Prog. Surf. Sci. **79**, 47–154 (2005)
32. L.M. Fang, X.T. Zu, Z.J. Li, S. Zhu, C.M. Liu, W.L. Zhou, J. Alloy. Compd. **454**, 261–267 (2008)
33. C-Y. Wang, D.W. Bahnemann, J.K. Dohrmann, Chem. Commun. **16**, 1539–1540 (2000)
34. S. Banerjee, M. Mandal, N. Gayathri, M. Sardar, Appl. Phys. Lett. **91**(18), 182501 (2007)
35. K. Potzger, J. Osten, A.A. Levin, A. Shalimov, G. Talut, H. Reuther, S. Arpaci, D. Burger, H. Schmidt, T. Nestler, D.C. Meyer, J. Magn. Magn. Mater. **323**, 1551–1562 (2011)
36. Q. Xu, H. Schmidt, S. Zhou, K. Potzger, M. Helm, H. Hochmuth, M. Lorenz, A. Setzer, P. Esquinazi, C. Meinecke, M. Grundmann, Appl. Phys. Lett. **92**, 082508 (2008)
37. J.M.D. Coey, P. Douvalis, B.C. Fitzgerald, M. Venkatesan, Appl. Phys. Lett. **84**, 1332–1334 (2004)